JACS
JOURNAL OF THE AMERICAN CHEMICAL SOCIETY
Article
pubs.acs.org/JACS

Rational Design of Charge-Transfer Interactions in Halogen-Bonded Co-crystals toward Versatile Solid-State Optoelectronics

Weigang Zhu,[†,‡] Renhui Zheng,[†] Yonggang Zhen,[†] Zhenyi Yu,[†,‡] Huanli Dong,*[,†] Hongbing Fu,[†] Qiang Shi,[†] and Wenping Hu*[,†,§]

[†]Institute of Chemistry, Chinese Academy of Sciences, Beijing 100190, P. R. China

[‡]University of Chinese Academy of Sciences, Beijing 100049, P. R. China

[§]Collaborative Innovation Center of Chemical Science and Engineering and School of Science, Tianjin University, Tianjin 300072, China

Supporting Information

ABSTRACT: Charge-transfer (CT) interactions between donor (D) and acceptor (A) groups, as well as CT exciton dynamics, play important roles in optoelectronic devices, such as organic solar cells, photodetectors, and light-emitting sources, which are not yet well understood. In this contribution, the self-assembly behavior, molecular stacking structure, CT interactions, density functional theory (DFT) calculations, and corresponding physicochemical properties of two similar halogen-bonded co-crystals are comprehensively investigated and compared, to construct an "assembly−structure−CT-property" relationship. Bpe-IFB wire-like crystals (where Bpe = 1,2-bis(4-pyridyl)ethylene and IFB = 1,3,5-trifluoro-2,4,6-triiodobenzene), packed in a segregated stacking form with CT ground and excited states, are measured to be quasi-one-dimensional (1D) semiconductors and show strong violet-blue photoluminescence (PL) from the lowest CT_1 excitons (Φ_{PL} = 26.1%), which can be confined and propagate oppositely along the 1D axial direction. In comparison, Bpe-F_4DIB block-like crystals (F_4DIB = 1,4-diiodotetrafluorobenzene), packed in a mixed stacking form without CT interactions, are determined to be insulators and exhibit unique white light emission and two-dimensional optical waveguide property. Surprisingly, it seems that the intrinsic spectroscopic states of Bpe and F_4DIB do not change after co-crystallization, which is also confirmed by theoretical calculations, thus offering a new design principle for white light emitting materials. More importantly, we show that the CT interactions in co-crystals are related to their molecular packing and can be triggered or suppressed by crystal engineering, which eventually leads to distinct optoelectronic properties. These results help us to rationally control the CT interactions in organic D−A systems by tuning the molecular stacking, toward the development of a fantastic "optoelectronic world".

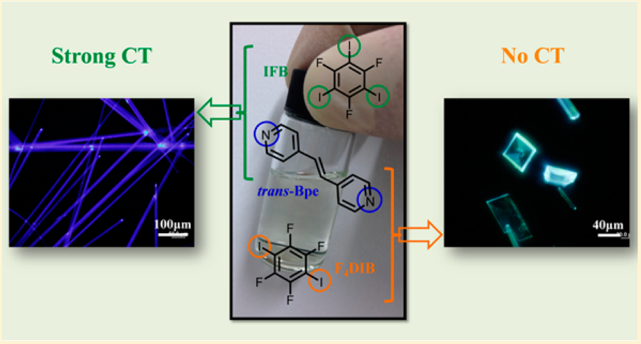

INTRODUCTION

Organic co-crystals formed with two or more different materials through intermolecular non-covalent interactions, such as $\pi-\pi$ interactions and hydrogen and halogen bonds, are gaining increasing research attention because of their applications in ambipolar charge transport,[1−3] photoconductivity,[4,5] photovoltaics,[6] ferroelectrics,[7,8] tunable light emitters,[9,10] nonlinear optics,[11,12] light-driven actuators,[13] liquid crystal materials,[14] and the drug industry.[15] More interestingly, the physicochemical properties of co-crystals are not simply the sum of molecular properties of the constituent compounds. For instance, Kim and co-workers[16] have demonstrated a "direct heavy atom effect" principle to design and make pure and color-tunable organic phosphors, the highest ambient phosphorescent quantum yield of which reaches up to 55%. In this regard, co-crystallization opens a door not only for synthesis of new multifunctional materials but also for exploration of novel physical and chemical phenomena. The optoelectronic properties of organic co-crystals have been focused on very recently,[17−23] though the first co-crystal "quinhydrone" was already discovered by Wöhler in 1844,[24] while the definition of "co-crystal" was given in and has been generally accepted since 2003.[25−27] This is partially because many challenges remain in this direction; one of them is to achieve effective co-crystallization.[28] As reported, there exist many strategies for co-crystal formation, including solution,[29] vapor-phase,[30] and mechanochemical techniques.[15] Among these methods, the solution-based approach is particularly important and most commonly used, because it is regarded as the simplest way to obtain organic co-crystals with uniform and regular morphology, which is convenient for further optoelectronic character-

Received: May 30, 2015
Published: July 30, 2015

DOI: 10.1021/jacs.5b05586
J. Am. Chem. Soc. 2015, 137, 11038−11046

ization. To apply this method for co-crystallization, some fundamental conditions, such as strong intermolecular interactions, planar molecular structure of donor (D) and acceptor (A) groups, and similar solubility of the D and A are essential. Since their discovery in 1863,[31] halogen bonds, showing a strong non-covalent interaction with excellent directionality, have been found to be more effective than hydrogen bonds[32] to control the construction of supramolecular architectures,[33] which is becoming a thriving tool for co-crystal engineering. Unfortunately, chemists and materials scientists have paid more attention to geometric design,[32,34−37] temperature-dependent molecular structure,[38] and liquid crystal engineering[14] in the supramolecular assembly of halogen-bonded systems rather than their co-crystal formation mechanism and optoelectronic properties in the past years. Because of this, halogen-bonded co-crystals are designed and prepared irrationally, and not well-explored,[9,10,20] resulting in large limitations in their optoelectronic functions and applications. Therefore, halogen bonding as an efficient co-crystallization strategy offers a powerful technique to explore the fantastic physicochemical properties of multi-component solid-state materials, urgently calling for a more rational preparation of halogen-bonded systems and comprehensive investigations of their optoelectronic properties.

Another problem is verifying the CT interaction in organic co-crystals and revealing its impact on physicochemical properties. Strictly speaking, there are two types of CT complexes: π and σ. The one drawing much more attention is the π CT complex, in which a π electron cloud largely delocalizes from a donor to an acceptor, resulting in a significant influence on bulk optoelectronic characteristics.[39−42] Typically, the halogen-bonded co-crystal is a σ complex, where the lone electron pair of an N atom donates to the halogen acceptor (n→σ* donation) to form a "halogen bond".[43,44] CT interactions involving π electrons in these co-crystals have been barely investigated, so little is known about their optoelectronic properties. For example, Yan and co-workers reported several halogen- and hydrogen-bonded co-crystals with tunable optical properties, and they attributed these changes to the formation of excimers,[9] and later J-aggregates,[10] which conflicts with the photoluminescence quantum yield (PLQY, Φ_{PL}) and lifetime data. As a matter of fact, the strong CT interactions in the ground state of organic co-crystals are of key importance to their molecular properties, such as photoconductivity[5] and photoluminescence,[45] and the CT degree can be easily detected by Raman and IR measurements,[46,47] while others are not.[48,49] D−A co-crystals with a neutral ground state but a CT excited state are also particularly attractive, because photoinduced CT happens when they are excited, and the generated singlet excitons change ultrafast to CT excitons, which is common but not well understood in organic photovoltaics.[50] In this sense, it is especially important to accurately confirm whether CT interactions exist in organic co-crystals, as well as to gain deeper insight into the influences of both CT interactions and the evolution of excitons on optoelectronic performance, which currently remain unclear.

With these considerations in mind, we herein select 1,2-bis(4-pyridyl)ethylene (*trans*-Bpe) and two halogenated co-formers, 1,3,5-trifluoro-2,4,6-triiodobenzene (IFB) and 1,4-diiodotetrafluorobenzene (F_4DIB) (Figure 1a), which can form 1:1 halogen complex crystals: Bpe-IFB co-crystal (BIC) and Bpe-F_4DIB co-crystal (BFC). We fully investigate and compare the self-assembly, crystal morphology, molecular stacking structure, CT interactions, and computational

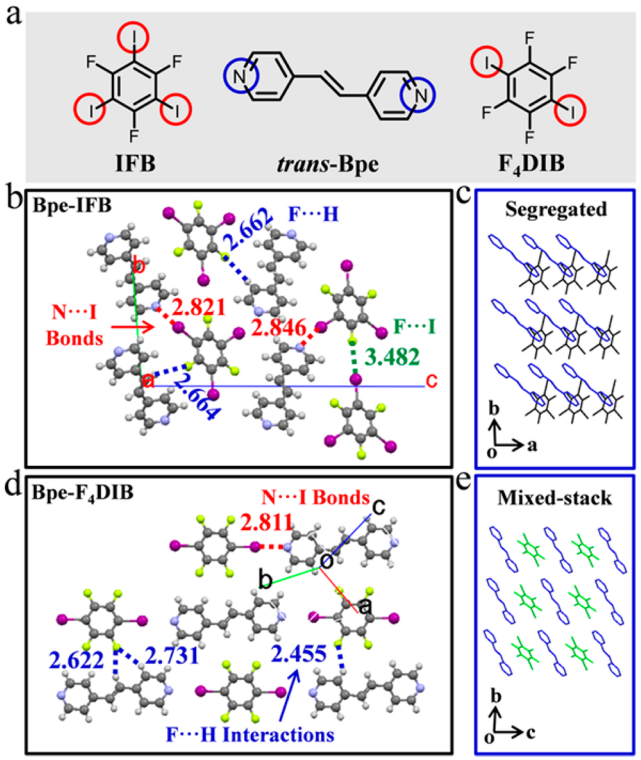

Figure 1. (a) Chemical structures of Bpe, IFB, and F_4DIB. Intermolecular interactions and molecular packing structures of (b) BIC and (d) BFC. Schematic diagrams of (c) segregated stacking in BIC and (e) mixed stacking in BFC.

calculations, as well as the corresponding spectroscopic, electric, and optical waveguide properties of these two types of co-crystals. Hence, the "assembly−structure−CT-property" relationship in these unique co-crystals is revealed and explored in-depth, and we demonstrate that the CT interactions in organic co-crystals can be modulated (triggered or suppressed) via a supramolecular crystal engineering strategy, which ultimately results in distinct optoelectronic performances. Notably, we attribute the selective appearance of CT interactions in segregated-stacking BICs to the π electron-rich character of Bpe columns, which promotes the CT process from donor Bpe to acceptor IFB, thus giving deeper understanding of the relationship among molecular packing structures, CT interactions, and optoelectronic characteristics of co-crystals.

EXPERIMENTAL SECTION

Materials and Chemicals. 1,2-Di(4-pyridyl)ethylene (*trans*-Bpe, CAS registry no. 13362-78-2, 97%+) was purchased from Sigma-Aldrich Co.; 1,3,5-trifluoro-2,4,6-triiodobenzene (IFB, CAS registry no. 84322-56-5, 97%) was purchased from Alfa Aesar Co.; and 1,4-diiodotetrafluorobenzene (F_4DIB, CAS registry no. 392-57-4, 98%) was purchased from J&K Co. All of them were used directly without further purification. Acetonitrile (CH_3CN, HPLC) and dichloromethane (CH_2Cl_2, HPLC) were purchased from Beijing Chemical Co., China. Deionized water (18.2 MΩ·cm^{-1}) was made by using a Milli-Q (Millipore) water purification system.

Co-crystal Growth and Characterization. BICs and BFCs were prepared by solution drop-casting. In a typical experiment, Bpe and IFB were mixed in a molar ratio of 1:1 and dissolved in acetonitrile solution, while Bpe and F_4DIB were dissolved in dichlormethane solution. The mixed solution was then directly dropped onto the substrate (glass or SiO_2/Si wafer), and co-crystals were observed after

DOI: 10.1021/jacs.5b05586
J. Am. Chem. Soc. 2015, 137, 11038−11046

the solvent evaporated completely. Transmission electron microscopy (TEM) and selected area electron diffraction (SAED) were performed using a JEOL JEM-1011 electron microscope at an acceleration of 100 kV to gain sufficient transmission. For preparation of TEM samples, the mixed solution was dropped onto the TEM grids, and co-crystals appeared in several minutes. The crystal structures were measured in an X-ray diffractometer (XRD, X-Pert, PANalytic, Netherlands) with Cu Kα radiation (40 kV, 30 mA). Raman spectra were collected on an inVia-Reflex Raman spectrometer (Renishaw, UK) excited with a 785 nm laser. Fourier transform infrared (FTIR) spectra were recorded on a TENSOR 27 instrument (Bruker, Germany). Electron spin resonance (ESR) spectroscopy was performed on a Bruker ESP 300 spectrometer (Bruker Co., Germany) with a resonance frequency of 9.78 GHz.

Morphology Predictions and Theoretical Calculations. The growth morphologies of co-crystals were calculated by using the Materials Studio software, based on the attachment energy theory. The molecular structure was first optimized on the basis of the experimental crystal structure. The geometric and energy calculations were performed using the Forcite and Morphology modules. For the DFT calculations, the molecular structures were not optimized first. The Mulliken atom charge, static dipole moment (SDM), lowest unoccupied molecular orbital (LUMO), and highest occupied molecular orbital (HOMO) of co-crystals in the ground state were calculated using the M06 density functional with the basis set LanL2DZ for the I atom and the basis set 6-31+G(d,p) for the other atoms. The absorption spectra, oscillator strength, and transition dipole moment (TDM) of the co-crystals were calculated by time-dependent density functional theory (TD-DFT) using the M06 density functional. All the computations were done within the Gaussian 09 program.[62]

Optical Characterization. Confocal laser scanning microscopy (CLSM) images were recorded on a glass substrate using an Olympus Research inverted system microscope (FV1000-IX81, Tokyo, Japan) equipped with a charge-coupled device (CCD, Olympus DP71, Tokyo, Japan) camera. The excitation source was a xenon lamp equipped with a band-pass filter (330−380 nm). The steady absorption spectra of crystals were recorded on a Cary 5000 UV−vis−NIR instrument (Varian, USA), and the PL spectra were collected on Horiba FluoroMax-4-NIR spectrophotometers. The PLQY (Φ_{PL}) was measured absolutely by using an integrating sphere. Microarea photoluminescence (μ-PL) spectra were collected on a homemade optical microscopy. The BICs were excited with a continuous-wave He−Cd laser (λ = 374 nm), while BFCs were excited with an argon ion laser (λ = 351 nm), and PL spectra were coupled into an optical fiber and collected using a liquid nitrogen cooled CCD (SPEC-10-400B/LbN, Roper Scientific) attached to a polychromator (Spectropro-550i, Acton). The PL lifetimes were detected with a streak camera (C5680, Hamamatsu Photonics), dispersed by a polychromator (250is, Chromex), with a spectral resolution of 1 nm and a time resolution of 10 ps.

Electrical Characterization. Si/SiO_2 wafers (SiO_2 300 nm thick, 10 nF cm^{-2}) were washed with deionized water, hot H_2SO_4:H_2O_2 (2:1) solution, deionized water, and isopropyl alcohol and dried by using a N_2 gun. Co-crystals were directly grown on the substrate by the solution drop-casting method. A glass substrate was used for growth of BFCs. To completely remove the solvent, co-crystals were put in a vacuum for 1 h. Gold electrodes (100 nm thick) were then fabricated on the crystals, using the "pick and paste" method. The device fabrication and measurement process were carried out with a Micromanipulator 6150 probe station. The current−voltage (I−V) curves were recorded by using a Keithley 4200 SCS analyzer, and all the measurements were conducted at room temperature in air.

RESULTS AND DISCUSSION

The BICs consist of Bpe molecular columns with a shorter intermolecular distance of 3.18 Å (Supporting Information, Figure S1b,c) compared with the Bpe crystal (3.67 Å, Figure S1f,g), implying strong π−π interactions. IFB molecular columns are formed by relatively weak π−π (3.54 Å, Figure S1d,e) and F···I interactions (3.48 Å), communicating with adjacent Bpe columns by two types of N···I halogen bonds (2.82 and 2.85 Å) and F···H interactions (2.66 Å), as displayed in Figure 1b. These intermolecular interactions, stretching along distinct directions, are responsible for the resulting segregated-stacking structure (Figure 1c). In sharp contrast, Bpe and F_4DIB molecules are connected by a N···I halogen bond (2.81 Å) to form linear molecular chains (Figure 1d), which later expand into a 2D molecular plane via three types of F···H interactions (2.46, 2.62, and 2.73 Å). These 2D molecular planes are then brought together by weak π−π interactions (3.64 Å, Figure S2) to form a unique mixed-stacking system (Figure 1e). Significantly different non-covalent interactions in two types of co-crystals may play important roles in the following molecular self-assembly.

Morphology predictions are performed by using Materials Studio software with the growth morphology algorithm. The calculation result depicted in Figure 2a reveals that BIC may

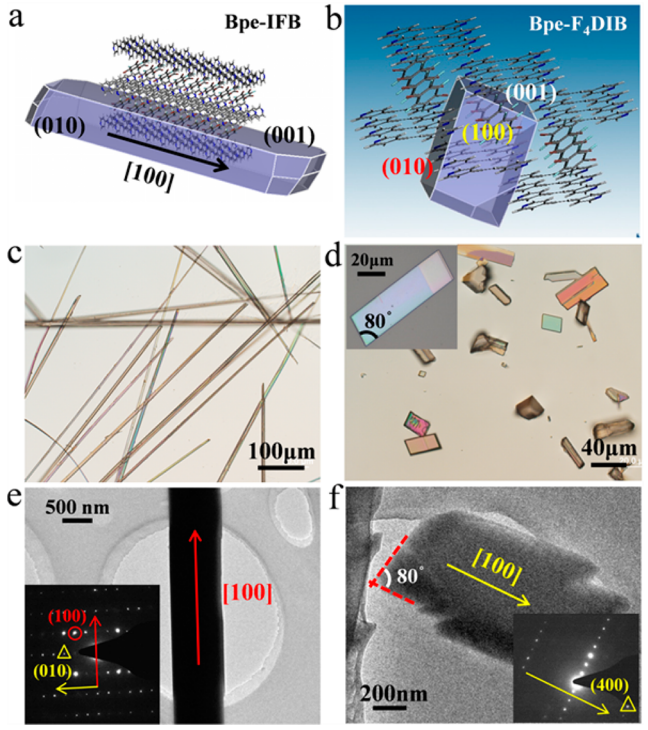

Figure 2. Predicted growth morphology of (a) BIC and (b) BFC. Optical images of (c) BICs and (d) BFCs obtained by solution drop-casting. TEM and SAED images of (e) BIC and (f) BFC.

grow along the [100] direction, and the lowest attachment energy for the (001) face (Figure S3) suggests it will be prominent in the crystal morphology. In comparison, BFCs may grow into block-like crystals (Figure 2b), and the attachment energy calculations (Figure S4d) indicate that any common crystal planes (such as (100), (010), and (001)) might appear to be dominant in the resulting bulk crystals. Despite the above discussions, BICs and BFCs are supramolecular prepared by drop-casting of mixed solution onto substrate, in which Bpe and co-former molecules recognize each other and self-assemble in an orderly way via non-covalent interactions from one to few and larger aggregates, initial nucleus to bulk molecular crystals, as shown in Figure 2c,d. Bpe and IFB molecules self-assemble into ultralong wires with a

DOI: 10.1021/jacs.5b05586
J. Am. Chem. Soc. 2015, 137, 11038−11046

width of hundreds of nanometers to several micrometers, uniformly distributed along the entire length, while Bpe and F_4DIB molecules aggregate into microblock crystals with various shapes (Figure S5). Both are distinctly different from single-component crystals obtained by the same solution method (Figures S6 and S7) and thus can be easily distinguished.

Figure 2e,f displays the TEM and SAED images of BIC and BFC, suggesting the two types of co-crystals are single-crystalline in nature. BIC belongs to the triclinic space group $P\bar{1}$,[43] with cell parameters of a = 4.73 Å, b = 9.07 Å, c = 22.60 Å, α = 94.53°, β = 93.22°, and γ = 92.32°, while Bpe and F_4DIB molecules self-assemble into the co-crystal[44] with cell parameters of a = 6.27 Å, b = 8.44 Å, c = 9.23 Å, α = 83.61°, β = 70.75°, and γ = 78.40°. Hence, the nice SAED pattern of individual BICs with similar d-spacing values of 4.67 and 9.0 Å and an intersection angle of 92° is indexed to the (100) and (010) planes, respectively. This indicates that the BIC wire is grown along the [100] direction, well in accord with the XRD measurement (Figure S8a), in which only the (002) peak is observed. Here we show that the morphology and structure of BICs are consistent with the Materials Studio software predictions, and the strong $\pi-\pi$ interaction between Bpe molecules is the main driving force for 1D self-assembly.

In stark contrast, more peaks appear in the XRD profile of BFCs (Figure S8b) because of its polymorphic nature. The observation of three types of crystal shapes (Figure S5) is consistent with the prediction results (Figure S4a–c). Specially, the b crystal plane is the most likely to be detected, as shown in the XRD result, corresponding to the (010) plane with the lowest attachment energy and the largest facet area in the calculation results (Figure S4d). The selected parallelogram-like BFC, with an intersection angle of 80° (Figure 2d), which possesses a better morphology than the others, is convenient for optoelectronic characterizations. As clearly confirmed in Figure 2f, it expands along the [100] direction. Thus, in this unique 2D molecular self-assembly (Figure S4a), C–F···H interactions are the main driving forces for the growth of (100), while the N···I halogen bonds are responsible for the growth along [010]. The above analysis and results therefore allow us to conclude that distinct non-covalent interactions between Bpe and two co-formers trigger different molecular self-assembly, resulting in diverse co-crystal morphologies with different molecular packing structures.

Raman (Figure S9) and IR spectra (Figure S10) are recorded to investigate the vibrational characteristics. Sharp bands in the Raman spectra indicate the co-crystals are highly crystalline and indeed composed of Bpe and co-former materials. The 158 cm^{-1} Raman band[20,51] (symmetric C–I stretching and ring elongation) of F_4DIB is shifted to 150 cm^{-1} after co-crystallization, while its 761 cm^{-1} IR band[51] (C–I antisym str) moves to 750 cm^{-1}, and the 1467 cm^{-1} IR band[52] (aryl semicircle stretch) changes to 1454 cm^{-1}. These observations clearly suggest that the C–I bond is lengthened and weakened as a consequence of n→σ^* donation and N···I halogen bond formation in BFCs. Additionally, the 943 cm^{-1} IR band[51] (C–F side-to-side stretch) of F_4DIB is shifted to 938 cm^{-1}, corresponding to the C–F···H interactions in BFCs. Similarly, the 179 cm^{-1} Raman band (C–I str) of IFB is red-shifted to 164 cm^{-1}, whereas its 1407 cm^{-1} IR band (ring stretch) moves to 1399 cm^{-1}, and the 1051 cm^{-1} IR band (C–F stretch) is shifted down to 1038 cm^{-1} in BICs. These changes after IFB co-crystallization are attributed to the N···I and F···H interactions. The formation of strong halogen bonds in two types of co-crystals is moreover reflected in the 3027 cm^{-1} IR band (C–H str) of Bpe, the intensity of which is largely weakened after co-crystallization.

With a deeper understanding of the effect of intermolecular interactions on molecular self-assembly, we then focused on the photophysical properties of co-crystals. Figure 3a,b depicts the

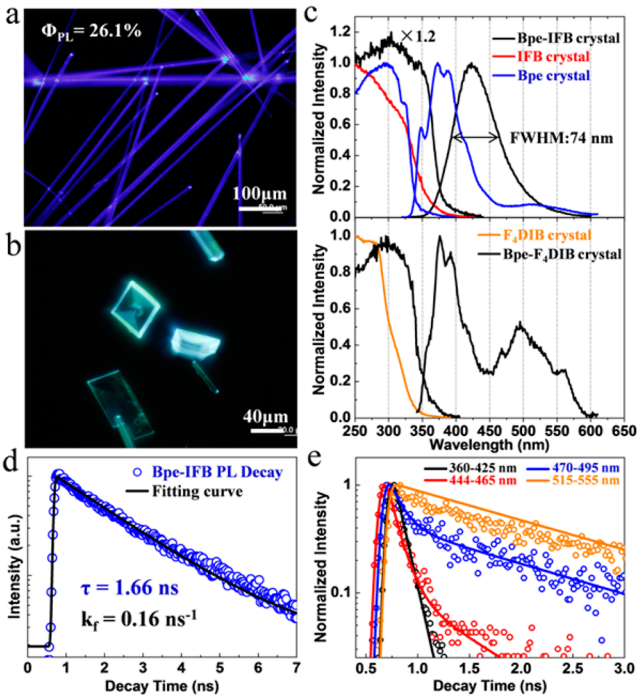

Figure 3. Photophysical properties of co-crystals. CLSM images of (a) BICs and (b) BFCs on the glass substrate under the excitation of an unfocused UV light (330–380 nm). (c) Absorption and PL spectra of Bpe, IFB, F_4DIB, Bpe-IFB, and Bpe-F_4DIB crystals on quartz slices. Time-resolved PL measurements of (d) BICs (monitored at 425 nm) and (e) BFCs. All the PL lifetime measurements were performed under the excitation of a 330 nm femtosecond laser.

CLSM images of BICs and BFCs. The BICs exhibit strong violet-blue luminescence with measured PLQY (Φ_{PL}) of 26.14%, while BFCs show unexpected white light emission (Figure S11). The extreme lightening at the tips or edges but not in the body of the co-crystals suggests their excellent self-waveguide properties. Moreover, the absorption and PL spectra of these two types of co-crystals were collected, as displayed in Figure 3c. The CIE chromaticity coordinates of BICs and BFCs (Figure S12) calculated from their PL spectra are (0.159, 0.084) and (0.258, 0.327), respectively. Compared with the individual component crystals, BICs exhibit two largely bathochromic-shifted absorptions at 326 and 354 nm (Figure S13), and a broad, structureless, red-shifted PL peaked at 425 nm, with the full width at half-maximum (fwhm) around 74 nm and a large Stokes shift of 4719 cm^{-1}, implying that they may originate from CT transitions. In contrast, the absorption and PL spectra of BFCs seem to retain the original values of single-component crystals (Figures 3c, S13, and S14).

To shed light on the nature of this interesting phenomenon and gain deeper insight into the excited states of co-crystals, the time-resolved PL measurements of BICs and BFCs were conducted, and the results are shown in Figure 3d,e. The PL of BICs peaking at 425 nm, with a lifetime (τ) around 1.66 ns, is

DOI: 10.1021/jacs.5b05586
J. Am. Chem. Soc. 2015, 137, 11038–11046

very different from that of Bpe crystals obtained via a similar solution method (Figure S15), demonstrating a distinct excited PL species. The radiation rate constant (k_f) of BICs is then calculated to be 0.16 ns^{-1} using the formula $k_f = \Phi_{PL}/\tau$, which is very close to the values of typical halogen-bonded co-crystals[9,10] and smaller than those of single-component crystals.[53,54] This relatively slow radiation implies its CT transition nature. For BFCs, PL decays at 360−425 nm with a lifetime of 0.10 ns, and a double-exponential decay of τ_1 = 0.10 ns (93%) and τ_2 = 0.71 ns (7%) is detected at 444−465 nm, while another double-exponential value of τ_1 = 0.12 ns (71.2%) and τ_2 = 1.55 ns (28.8%) is fitted at 470−495 nm, and 1.59 ns is monitored at 515−555 nm (Figure 3e). We note that the PL decay times of BFCs almost do not change at all (Figure S15) as compared with those of Bpe crystals, showing that incorporation of F_4DIB molecules into the co-crystals does not change the intrinsic spectroscopic states of Bpe. The exception is that monitored at 470−555 nm of BFCs, in which a shortened lifetime (1.55 ns) is observed. This reduction in the PL lifetime, compared with that monitored at 485−565 nm (3.95 ns) from Bpe crystals, is attributed to the introduction of the acceptor molecules F_4DIB into this system, which probably increases the nonradiative pathways from the corresponding excited state of Bpe. The above phenomenon observed in the BFC system, to the best of our knowledge, is surprising and has been little reported, since co-crystallization alters the original molecular packing structure and is regarded as an advanced strategy to tune the optical properties of solid materials, as proposed recently.[9,10]

Interestingly, incorporating similar co-formers into co-crystal systems leads to different intermolecular interactions, molecular self-assembly behaviors, crystal morphologies, and molecular stacking structures, as well as distinct photophysical properties. We think that the broad, structureless, and red-shifted PL from BICs with longer PL lifetime (1.66 ns) may be attributed to the CT interactions from donor Bpe to acceptor IFB, which do not appear in BFCs, resulting in a white-light emission simply made up of those from single-component crystals. However, as shown above, the CT interactions of co-crystals cannot be detected in Raman (Figure S9) and IR spectra (Figure S10), which is significantly different from the case of TCNQ-based co-crystals.[55] The CT nature of BICs in the ground state is first experimentally confirmed by ESR measurements (Figure S16). A relatively weak but sharp signal appears centered at the magnetic field of 3481 G, indicating unpaired electrons exist in the co-crystals. The *g*-factor is calculated to be 2.0045 according to the ESR theory, which is similar to that of free electron (2.0023), revealing the CT interactions between Bpe and IFB. Note that we did not observe any ESR signals in Bpe or IFB powder.

The CT interactions and photophysical properties of co-crystals are completely revealed by DFT calculations (Figure 4). The Mulliken atom charge of +0.106 on the IFB moiety with a SDM of 0.78 D, pointing to the IFB molecule (Figure S17a), and the calculated LUMO and HOMO of the BICs (Figure 4a) confirm the CT interactions in the ground state. In contrast, the smaller value of the Mulliken atom charge (0.036) and the vector of SDM parallel to the molecules (Figure S17b) in BFCs indicate almost no CT interactions between Bpe and F_4DIB. This is further verified by the calculated LUMO and HOMO (Figure 4b), both of which are nearly completely distributed on the Bpe moiety. The absorption spectra of co-crystals are calculated using TD-DFT, and the electronic

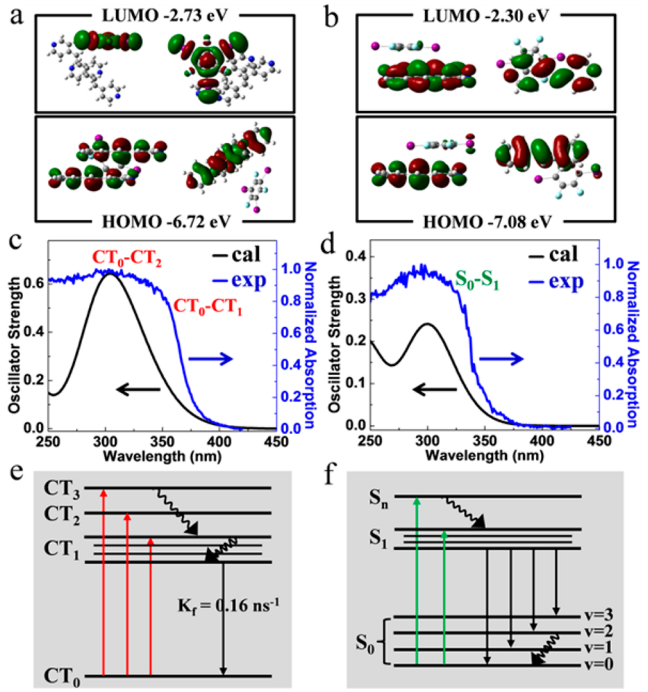

Figure 4. Molecular orbital diagrams of (a) BIC and (b) BFC as calculated by DFT. Absorption spectra calculated by TD-DFT (black curve) and experimental result (blue curve) for (c) BICs and (d) BFCs, and corresponding Jablonski diagrams (e,f).

transitions are assigned as displayed in Figures 4c,d and S18, and Tables S1 and S2.

For the BICs, the lowest $CT_0 \rightarrow CT_1$ transition is from the HOMO→LUMO excitation, and the energy of this transition, calculated as 361.4 nm (3.43 eV) with an oscillator strength (*f*) of 0.0021, is well in accord with the experimental results (354 nm, 3.50 eV).[56] The corresponding TDM, with a value of 0.4 D (Figure S19), displays its vector nearly perpendicular to the Bpe molecular columns. Similarly, the observed 326 nm (3.80 eV) absorption is attributed to the $CT_0 \rightarrow CT_2$ transition (calculated as 328.3 nm, 3.78 eV), which is mainly from the HOMO→LUMO+2 excitation (47.3%), while the 258 nm (4.81 eV) peak is assigned to the $CT_0 \rightarrow CT_3$ transition (calculated as 257.5 nm, 4.81 eV). Moreover, the strong PL of BICs is from the lowest CT_1 state (CT_1 excitons), since a nice mirror-image relationship between absorption and PL spectra has been observed. For the BFCs, the calculated absorption spectra also agree well with the experiments (Figure 4d), and the calculated molecular orbitals and energy levels are almost the same as those of Bpe crystals (Figure S20). This agrees with the previous discussions of photophyscial properties of Bpe and BFC, which have concluded that the spectroscopic states of Bpe and F_4DIB do not change after co-crystallization, though the molecular packing structure of Bpe is largely altered in the co-crystals. In this regard, the experimental absorption of 325 nm (3.82 eV) for BFCs can be attributed to the $S_0 \rightarrow S_1$ transition of Bpe, while the PL of BFCs is near that of Bpe crystals, the optical characteristics of which are also theoretically revealed, as illustrated in Figure S21 and Table S3.

The experimental and theoretical evidence helps us to draw the corresponding Jablonski diagrams of the two types of co-crystals, as exhibited in Figure 4e,f. In BICs, electronic transitions happen from the CT_0 ground state to CT_n excited states when photons are absorbed and then relax (internal

DOI: 10.1021/jacs.5b05586
J. Am. Chem. Soc. 2015, 137, 11038−11046

conversion) to the CT_1 state, and via a large molecular configuration change (Stokes shift) to fluoresce with radiation rate constant $k_f = 0.16\ ns^{-1}$. The k_f value is larger than those of TCNB-based co-crystals[45] but similar to those of halogen-bonded co-crystals.[9] In comparison, when BFCs are excited, electronic transitions happen between singlet states, with fluorescence mainly from the lowest S_1 state. The Bpe component in BFCs plays a more important role than F_4DIB, which contributes to the absorption spectrum of BFCs but shows extremely weak fluorescence (Figure S14).

The selective appearance of CT interactions in two types of co-crystals grown from similar co-former molecules is surprising. It is generally accepted that the CT degree is usually significant in the co-crystals with segregated stacking and relatively smaller in the co-crystals with mixed stacking. The co-crystals with strong CT interactions and significant CT degree in the ground state prefer to pack in a segregated form in order to stabilize the ionic D−A system. However, the basic reason for this still remains unclear. Here we propose that the CT interactions in organic co-crystals can be selectively triggered or suppressed by different molecular packing structures, and the π electron cloud delocalized in the Bpe columns (π-electron-rich) promotes the CT process from Bpe to IFB (Figure S22). In comparison, Bpe molecules are dispersed in BFCs, leading to π-electron-deficient circumstances and weak CT interactions between Bpe and F_4DIB. These results give a convincing explanation and deeper insight into the relationship between molecular packing structures and CT interactions in organic co-crystals.

The electric conductivity (σ) of the two types of co-crystals is also examined. In a typical experiment, BIC wires were grown on the Si/SiO_2 wafer by directly drop-casting of mixed solution (Figure 5a), followed by the fabrication of two-terminal microscale devices, using the "pick and paste" technique.[57] Figure 5b displays the measured $I-V$ characteristics of individual BIC at room temperature. The linear relationship suggests that the $I-V$ behavior of BIC obeys Ohm's law at low applied voltage, and a nearly ohmic contact exists between the crystal and electrodes. Note that the $I-V$ curve does not go through the origin of the coordinates, and this might be due to the noise current. Using the formula

$$\sigma = \frac{1}{\rho} = \frac{1}{R(S/L)} = \frac{L}{RS} = \frac{L}{RWH}$$

where σ, ρ, and R are the electric conductivity, resistivity, and resistance values of the wire, and S, L, W, and H are the area, length of device channel, and width and height of the crystal, respectively, the electric conductivity of BIC is calculated to be $\sigma = 1.42 \times 10^{-6}\ \Omega^{-1}\ m^{-1}$, suggesting that BIC has quasi-1D semiconductor nature (along the [100] direction). More than 20 devices were measured in our experiments, and the results ranges from $\sigma = 8.08 \times 10^{-7}$ to $8.73 \times 10^{-6}\ \Omega^{-1}\ m^{-1}$. Note that light-emitting co-crystals exhibiting electric conductivity are little reported, and most of them are insulators.[58,59] On the other hand, BFCs were grown on the substrate (Figure 5c) and fabricated similarly to the two-terminal devices, which were eventually confirmed to be insulators (Figure 5d).

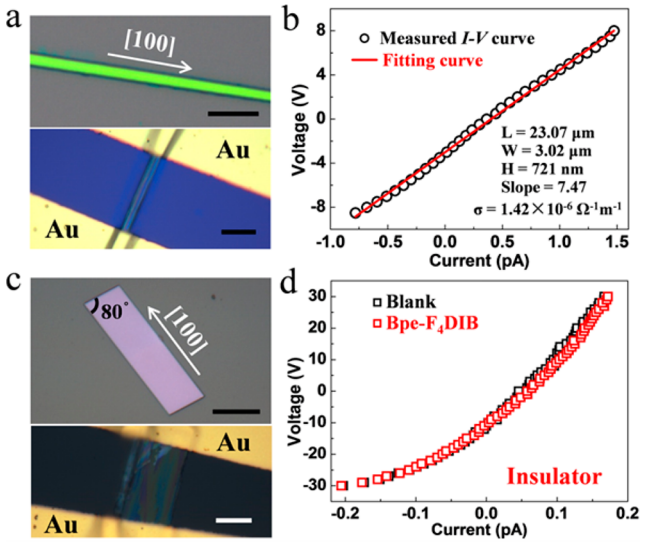

Figure 5. Electric conductivity of co-crystals. Optical images of (a) BIC on the Si/SiO_2 wafer (upper section) and wire-based device (bottom section), and of (c) BFC on a glass substrate (upper section) and microblock-based device (bottom section). The scale bars are 10 μm. (b) Measured current−voltage ($I-V$) curve and corresponding fitting line for BIC. (d) Measured $I-V$ curve for BFC.

Therefore, the Bpe-IFB CT co-crystal with segregated-stacking structure is determined to be a semiconductor, while the BFC packed in a mixed-stacking structure without CT interactions is measured to be an insulator. This is consistent with the fact that the electric conductivity of a co-crystal is related to its CT degree, as discussed in previous reports and generally accepted.[60] In this regard, the electric conductivity result also verifies the selective appearance of CT interactions in the two types of co-crystals. Besides this, we propose that the strong $\pi-\pi$ interactions (3.18 Å) in the Bpe columns ([100] direction) in BICs are also responsible for the measured electric conductivity, while that is not the case in BFCs.

The two types of halogen-bonded co-crystals with different molecular stacking forms, obtained from distinct molecular self-assembly processes, show different photophysical and electric characteristics due to the selective appearance of CT interactions, arousing our interests in further investigating their optical waveguide properties. In a typical experiment, spatially resolved PL imaging and spectroscopy measurements were performed on a homemade system (Figure S23). μ-PL spectra of co-crystals were collected as shown in Figure 6a,b. Compared with their steady PL spectra, the μ-PL spectra of the two types of co-crystals are changed and red-shifted, which may be attributed to the micro-cavity effect and re-absorption. Moreover, when the excitation 374 nm picosecond laser beam is focused on an individual BIC, the generated photons are confined, propagate in opposite ways, and out-couple at the tips in this 1D optical waveguide. The PL intensity collected from the tip (I_{tip}) gradually decreases (Figure 6c) when the excitation laser spot is moved to increase the optical propagation distance. The PL intensity of the excitation spot (I_{body}) was also collected, and the ratio I_{tip}/I_{body} shows a single-exponential decay against propagation distance (Figure 6d), which indicates the active nature of the optical waveguide. This decay curve can be fitted using the function

$$\frac{I_{tip}}{I_{body}} = A\ \exp(-RD)$$

where A and D are a constant and the optical propagation distance, respectively. Thus, the optical loss coefficient (R) of BIC is calculated to be 0.19 dB μm^{-1} at 440 nm, which is

DOI: 10.1021/jacs.5b05586
J. Am. Chem. Soc. 2015, 137, 11038−11046

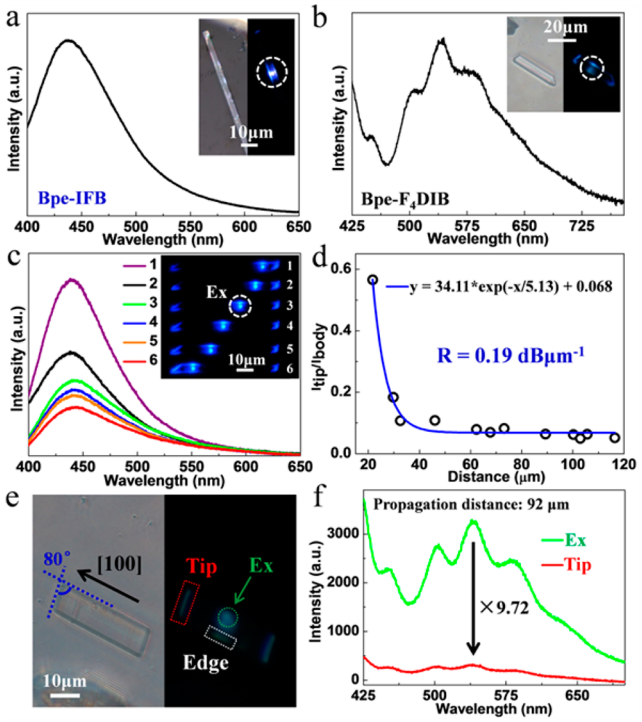

Figure 6. Optical waveguide of co-crystals. μ-PL spectra of individual (a) BIC and (b) BFC. Insets are corresponding bright-field and PL images. (c) Spatially resolved PL spectra collected from the tip of the wire when the excitation spot was moved. Inset shows the PL images of individual BIC excited at different positions. (d) Ratio of PL intensity, I_{tip}/I_{body}, against the propagation distance D. The curves were fitted by an exponential decay function. (e) Typical bright-field and PL images of a micro-block excited by a 351 nm laser. (f) Typical μ-PL spectra obtained from the excitation spot and tip of individual BFC.

comparable to those of organic crystals with excellent optical waveguide properties.[61] In contrast, under the excitation of a 351 nm laser, the excited white PL can propagate parallel to the glass substrate in an individual BFC along two distinct directions and out-couple at its tip and edge, exhibiting the unique 2D optical waveguide property (Figure 6e). Typically, for a long propagation distance in BFC, the intensity of white PL does not decrease so much (Figure 6f). Significantly, the BFC is the first reported co-crystal with 2D morphology to serve as an efficient 2D white light waveguide. Generally, when a molecular crystal serves as an optical waveguide, the optical propagation directions are mainly decided by its crystal morphology, while the optical propagation loss coefficient R is related to the material itself and the crystal quality. Hence, the two types of co-crystals with distinct morphologies exhibit different optical waveguide behaviors, further confirming that rational design of the intermolecular interactions and control of the molecular self-assembly are essential to obtain the crystals with the desired shapes and photonic functions.

CONCLUSIONS

Two types of supramolecular halogen-bonded co-crystals are prepared from Bpe and two similar co-former molecules, followed by in-depth structural, spectroscopic, theoretical, electronic, and photonic characterizations, and the results are summarized in Table 1. The analyses and discussions in this work allow us to conclude the following:

(1) The $\pi-\pi$ interaction in BICs is the main driving force for 1D self-assembly, resulting in ultralong wires with segregated stacking, while Bpe and F_4DIB prefer to undergo 2D self-assembly driven by C–F···H and N···I interactions to form bulk blocks with mixed stacking. This provides a reference for further rational design and preparation of halogen-bonded co-crystals using supramolecular strategies.

(2) The Bpe-IFB CT wires give efficient violet-blue PL (Φ_{PL} = 26.1%) with a typical radiation rate constant k_f = 0.16 ns^{-1}, which is from the lowest CT_1 state (CT_1 excitons). Surprisingly, the BFCs without CT interactions exhibit unique white light emission, which is made up of those from individual component crystals with almost the same PL lifetime, indicating that the intrinsic spectroscopic states of Bpe and F_4DIB indeed do not change after co-crystallization. This important result provides a new design principle for achieving white-light-emitting materials.

(3) The appearance of CT interactions in segregated-stacking BICs but not in mixed-stacking BFCs is also completely confirmed by DFT calculations. The absorption spectra and electronic transitions of the two types of co-crystals are calculated and assigned, in good accord with the experiments. Moreover, the calculated energy levels of Bpe crystals and BFCs are similar, and this is consistent with the observation that the BFCs retain the intrinsic spectroscopic states of Bpe and F_4DIB crystals. After verifying the CT interactions experimentally and theoretically, we propose that the π electron-rich circumstances in Bpe columns of BICs promote the CT process from donor Bpe to acceptor IFB. This suggests that CT interactions in co-crystals are related to their molecular packing structures and can be modulated (selectively triggered or suppressed) by crystal engineering. Impressively, it gives a deeper understanding of the relationship between molecular packing structures and CT interactions of organic co-crystals.

(4) The Bpe-IFB CT co-crystals are determined to be quasi-1D semiconductor, whereas BFCs without CT interactions are measured to be insulators. Both of the CT interactions and strong $\pi-\pi$ interactions along the [100] direction in BICs are responsible for its measured electric conductivity, further verifying the significant effect of CT interactions on optoelectronic properties.

(5) The distinct PL propagation behaviors in two types of co-crystals suggest that the optical waveguide property of molecular crystal is partially morphology-dependent. Thus, it is important to conduct the molecular self-assembly in a controlled manner to obtain crystals with the desired shapes and photonic functions.

Table 1. Molecular Self-Assembly Behavior and Optoelectronic Properties of BICs and BFCs

molecules	self-assembly manner	driving force	co-crystal morphology	molecular stacking	emission	CT	conductivity, Ω^{-1} m^{-1}	waveguide, dB μm^{-1}
Bpe, IFB	1D	$\pi-\pi$	wire-like	segregated	violet-blue	yes	1.42×10^{-6}	1D, 0.19
Bpe, F_4DIB	2D	N···I, C–F···H	block-like	mixed	white light	no	insulator	2D

DOI: 10.1021/jacs.5b05586
J. Am. Chem. Soc. 2015, 137, 11038–11046

The "assembly−structure−CT-property" relationship in halogen-bonded co-crystals, as described above, helps us to gain a deeper understanding of the correlations between molecular stacking structure, CT interactions, and optoelectronic characteristics of organic D−A systems, and opens up a rational way to design and efficiently synthesize a broad class of novel functional organic co-crystal materials. Further related research, underway in our group, will focus on measuring the CT degree of halogen-bonded co-crystals in the ground state, the basic reason why some co-crystals show spectroscopic behaviors similar to those of single-component crystals, and the exciton dynamics in co-crystal optoelectronic devices.

■ ASSOCIATED CONTENT

Supporting Information

The Supporting Information is available free of charge on the ACS Publications website at DOI: 10.1021/jacs.5b05586.

Molecular packing structures of crystals; morphology predictions of co-crystals; morphology of Bpe, IFB, F_4DIB, Bpe-IFB, and Bpe-F_4DIB crystals; XRD results; Raman and FTIR spectra; PL images of BFCs; CIE coordinates of co-crystals; absorption spectra of crystals; PL spectrum of F_4DIB crystals; PL lifetime measurements of crystals; ESR results; calculated SDM, Mulliken atom charges, absorption spectra, vertical transition energies and TDM of co-crystals, and energy levels; spectroscopic and theoretical study of Bpe; relationship between molecular packing structures and CT interactions; homemade platform for micro-area optical characterizations; and calculated excitation energies and oscillator strength of crystals (PDF)

■ AUTHOR INFORMATION

Corresponding Authors

*huwp@iccas.ac.cn

*dhl522@iccas.ac.cn

Notes

The authors declare no competing financial interest.

■ ACKNOWLEDGMENTS

The authors sincerely thank Dr. Jianyao Zheng and Dr. Yishi Wu for discussions and suggestions. They also acknowledge Dr. Yishi Wu for help with PL lifetime measurements, Cong Wei and Prof. Yongsheng Zhao for help with optical waveguide characterizations, Wenchao Zhao for the height analysis of co-crystals, Zongrui Wang for help with TEM characterizations, and Dr. Libo Du and Prof. Yang Liu for the ESR measurements. This work was supported by National Natural Science Foundation of China (91222203, 91233205, 51222306, 61201105, 91027043, 91433115, 51303185, 21473222, TRR61), the Ministry of Science and Technology of China (2011CB808400, 2011CB932300, 2013CB933403, 2013-CB933500, 2014CB643600), and the Chinese Academy of Sciences (XDB12020300).

■ REFERENCES

(1) Qin, Y.; Zhang, J.; Zheng, X.; Geng, H.; Zhao, G.; Xu, W.; Hu, W.; Shuai, Z.; Zhu, D. *Adv. Mater.* **2014**, *26*, 4093.

(2) Zhang, J.; Tan, J. H.; Ma, Z. Y.; Xu, W.; Zhao, G. Y.; Geng, H.; Di, C. A.; Hu, W. P.; Shuai, Z. G.; Singh, K.; Zhu, D. B. *J. Am. Chem. Soc.* **2013**, *135*, 558.

(3) Zhang, J.; Geng, H.; Virk, T. S.; Zhao, Y.; Tan, J. H.; Di, C. A.; Xu, W.; Singh, K.; Hu, W. P.; Shuai, Z. G.; Liu, Y. Q.; Zhu, D. B. *Adv. Mater.* **2012**, *24*, 2603.

(4) Tsutsumi, J. y.; Yamada, T.; Matsui, H.; Haas, S.; Hasegawa, T. *Phys. Rev. Lett.* **2010**, *105*, 226601.

(5) Vincent, V. M.; Wright, J. D. *J. Chem. Soc., Faraday Trans. 1* **1974**, *70*, 58.

(6) Kang, S. J.; Ahn, S.; Kim, J. B.; Schenck, C.; Hiszpanski, A. M.; Oh, S.; Schiros, T.; Loo, Y.-L.; Nuckolls, C. *J. Am. Chem. Soc.* **2013**, *135*, 2207.

(7) Horiuchi, S.; Ishii, F.; Kumai, R.; Okimoto, Y.; Tachibana, H.; Nagaosa, N.; Tokura, Y. *Nat. Mater.* **2005**, *4*, 163.

(8) Tayi, A. S.; Shveyd, A. K.; Sue, A. C. H.; Szarko, J. M.; Rolczynski, B. S.; Cao, D.; Kennedy, T. J.; Sarjeant, A. A.; Stern, C. L.; Paxton, W. F.; Wu, W.; Dey, S. K.; Fahrenbach, A. C.; Guest, J. R.; Mohseni, H.; Chen, L. X.; Wang, K. L.; Stoddart, J. F.; Stupp, S. I. *Nature* **2012**, *488*, 485.

(9) Yan, D.; Delori, A.; Lloyd, G. O.; Friščić, T.; Day, G. M.; Jones, W.; Lu, J.; Wei, M.; Evans, D. G.; Duan, X. *Angew. Chem., Int. Ed.* **2011**, *50*, 12483.

(10) Yan, D.; Yang, H.; Meng, Q.; Lin, H.; Wei, M. *Adv. Funct. Mater.* **2014**, *24*, 587.

(11) Bosshard, C.; Wong, M. S.; Pan, F.; Günter, P.; Gramlich, V. *Adv. Mater.* **1997**, *9*, 554.

(12) Pan, F.; Wong, M. S.; Gramlich, V.; Bosshard, C.; Günter, P. *J. Am. Chem. Soc.* **1996**, *118*, 6315.

(13) Morimoto, M.; Irie, M. *J. Am. Chem. Soc.* **2010**, *132*, 14172.

(14) Nguyen, H. L.; Horton, P. N.; Hursthouse, M. B.; Legon, A. C.; Bruce, D. W. *J. Am. Chem. Soc.* **2004**, *126*, 16.

(15) Braga, D.; Maini, L.; Grepioni, F. *Chem. Soc. Rev.* **2013**, *42*, 7638.

(16) Bolton, O.; Lee, K.; Kim, H.-J.; Lin, K. Y.; Kim, J. *Nat. Chem.* **2011**, *3*, 207.

(17) Horiuchi, S.; Hasegawa, T.; Tokura, Y. *J. Phys. Soc. Jpn.* **2006**, *75*, 051016.

(18) Goetz, K. P.; Vermeulen, D.; Payne, M. E.; Kloc, C.; McNeil, L. E.; Jurchescu, O. D. *J. Mater. Chem. C* **2014**, *2*, 3065.

(19) Lei, Y. L.; Liao, L. S.; Lee, S. T. *J. Am. Chem. Soc.* **2013**, *135*, 3744.

(20) Ventura, B.; Bertocco, A.; Braga, D.; Catalano, L.; d'Agostino, S.; Grepioni, F.; Taddei, P. *J. Phys. Chem. C* **2014**, *118*, 18646.

(21) Wakahara, T.; D'Angelo, P.; Miyazawa, K. i.; Nemoto, Y.; Ito, O.; Tanigaki, N.; Bradley, D. D. C.; Anthopoulos, T. D. *J. Am. Chem. Soc.* **2012**, *134*, 7204.

(22) Wakahara, T.; Sathish, M.; Miyazawa, K. i.; Hu, C. P.; Tateyama, Y.; Nemoto, Y.; Sasaki, T.; Ito, O. *J. Am. Chem. Soc.* **2009**, *131*, 9940.

(23) Zhu, W.; Zhen, Y.; Dong, H.; Fu, H.; Hu, W. *Prog. Chem.* **2014**, *26*, 1292.

(24) Wöhler, F. *Annalen* **1844**, *51*, 153.

(25) Aakeroy, C. B.; Salmon, D. J. *CrystEngComm* **2005**, *7*, 439.

(26) Desiraju, G. R. *CrystEngComm* **2003**, *5*, 466.

(27) Dunitz, J. D. *CrystEngComm* **2003**, *5*, 506.

(28) Wuest, J. D. *Nat. Chem.* **2012**, *4*, 74.

(29) Lei, Y. L.; Jin, Y.; Zhou, D. Y.; Gu, W.; Shi, X. B.; Liao, L. S.; Lee, S.-T. *Adv. Mater.* **2012**, *24*, 5345.

(30) Black, H. T.; Perepichka, D. F. *Angew. Chem., Int. Ed.* **2014**, *53*, 2138.

(31) Guthrie, F. *J. Chem. Soc.* **1863**, *16*, 239.

(32) Fan, E.; Vicent, C.; Geib, S. J.; Hamilton, A. D. *Chem. Mater.* **1994**, *6*, 1113.

(33) Metrangolo, P.; Resnati, G. *Chem. - Eur. J.* **2001**, *7*, 2511.

(34) Amico, V.; Meille, S. V.; Corradi, E.; Messina, M. T.; Resnati, G. *J. Am. Chem. Soc.* **1998**, *120*, 8261.

(35) Allen, F. H.; Goud, B. S.; Hoy, V. J.; Howard, J. A. K.; Desiraju, G. R. *J. Chem. Soc., Chem. Commun.* **1994**, 2729.

(36) Reddy, D. S.; Craig, D. C.; Rae, A. D.; Desiraju, G. R. *J. Chem. Soc., Chem. Commun.* **1993**, 1737.

(37) Zheng, Q.-N.; Liu, X.-H.; Chen, T.; Yan, H.-J.; Cook, T.; Wang, D.; Stang, P. J.; Wan, L.-J. *J. Am. Chem. Soc.* **2015**, *137*, 6128.

DOI: 10.1021/jacs.5b05586
J. Am. Chem. Soc. 2015, 137, 11038−11046

(38) Forni, A.; Metrangolo, P.; Pilati, T.; Resnati, G. *Cryst. Growth Des.* **2004**, *4*, 291.
(39) Das, A.; Ghosh, S. *Angew. Chem., Int. Ed.* **2014**, *53*, 2038.
(40) Saito, G.; Yoshida, Y. *Bull. Chem. Soc. Jpn.* **2007**, *80*, 1.
(41) Shibaeva, R. P.; Yagubskii, E. B. *Chem. Rev.* **2004**, *104*, 5347.
(42) Kumar, M.; Venkata Rao, K.; George, S. J. *Phys. Chem. Chem. Phys.* **2014**, *16*, 1300.
(43) Lucassen, A. C. B.; Karton, A.; Leitus, G.; Shimon, L. J. W.; Martin, J. M. L.; van der Boom, M. E. *Cryst. Growth Des.* **2007**, *7*, 386.
(44) Walsh, R. B.; Padgett, C. W.; Metrangolo, P.; Resnati, G.; Hanks, T. W.; Pennington, W. T. *Cryst. Growth Des.* **2001**, *1*, 165.
(45) Dillon, R. J.; Bardeen, C. J. *J. Phys. Chem. A* **2011**, *115*, 1627.
(46) Kistenmacher, T. J.; Emge, T. J.; Bloch, A. N.; Cowan, D. O. *Acta Crystallogr., Sect. B: Struct. Crystallogr. Cryst. Chem.* **1982**, *38*, 1193.
(47) Chi, X.; Besnard, C.; Thorsmølle, V. K.; Butko, V. Y.; Taylor, A. J.; Siegrist, T.; Ramirez, A. P. *Chem. Mater.* **2004**, *16*, 5751.
(48) Macfarlane, R. M.; Ushioda, S. *J. Chem. Phys.* **1977**, *67*, 3214.
(49) Bandoli, G.; Lunardi, G.; Clemente, D. A. *J. Crystallogr. Spectrosc. Res.* **1993**, *23*, 1.
(50) Rao, A.; Chow, P. C. Y.; Gelinas, S.; Schlenker, C. W.; Li, C.-Z.; Yip, H.-L.; Jen, A. K. Y.; Ginger, D. S.; Friend, R. H. *Nature* **2013**, *500*, 435.
(51) Hanson, G. R.; Jensen, P.; McMurtrie, J.; Rintoul, L.; Micallef, A. S. *Chem. - Eur. J.* **2009**, *15*, 4156.
(52) Gao, H. Y.; Shen, Q. J.; Zhao, X. R.; Yan, X. Q.; Pang, X.; Jin, W. J. *J. Mater. Chem.* **2012**, *22*, 5336.
(53) Xu, Z. Z.; Liao, Q.; Shi, Q.; Zhang, H. L.; Yao, J. N.; Fu, H. B. *Adv. Mater.* **2012**, *24*, OP216.
(54) Zhang, J.; Xu, B.; Chen, J.; Ma, S.; Dong, Y.; Wang, L.; Li, B.; Ye, L.; Tian, W. *Adv. Mater.* **2014**, *26*, 739.
(55) Van Duyne, R. P.; Cape, T. W.; Suchanski, M. R.; Siedle, A. R. *J. Phys. Chem.* **1986**, *90*, 739.
(56) Park, S. K.; Varghese, S.; Kim, J. H.; Yoon, S.-J.; Kwon, O. K.; An, B.-K.; Gierschner, J.; Park, S. Y. *J. Am. Chem. Soc.* **2013**, *135*, 4757.
(57) Tang, Q.; Li, H.; He, M.; Hu, W.; Liu, C.; Chen, K.; Wang, C.; Liu, Y.; Zhu, D. *Adv. Mater.* **2006**, *18*, 65.
(58) Samoc, M.; Williams, D. F. *J. Chem. Phys.* **1983**, *78*, 1924.
(59) Miniewicz, A.; Samoc, M.; Williams, D. F. *Mol. Cryst. Liq. Cryst.* **1984**, *111*, 199.
(60) Torrance, J. B. *Acc. Chem. Res.* **1979**, *12*, 79.
(61) Yao, W.; Yan, Y.; Xue, L.; Zhang, C.; Li, G.; Zheng, Q.; Zhao, Y. S.; Jiang, H.; Yao, J. *Angew. Chem., Int. Ed.* **2013**, *52*, 8713.
(62) Frisch, M. J.; Trucks, G. W.; Schlegel, H. B.; Scuseria, G. E.; Robb, M. A.; Cheeseman, J. R.; Scalmani, G.; Barone, V.; Mennucci, B.; Petersson, G. A.; Nakatsuji, H.; Caricato, M.; Li, X.; Hratchian, H. P.; Izmaylov, A. F.; Bloino, J.; Zheng, G.; Sonnenberg, J. L.; Hada, M.; Ehara, M.; Toyota, K.; Fukuda, R.; Hasegawa, J.; Ishida, M.; Nakajima, T.; Honda, Y.; Kitao, O.; Nakai, H.; Vreven, T.; Montgomery, J. A., Jr.; Peralta, J. E.; Ogliaro, F.; Bearpark, M.; Heyd, J. J.; Brothers, E.; Kudin, K. N.; Staroverov, V. N.; Kobayashi, R.; Normand, J.; Raghavachari, K.; Rendell, A.; Burant, J. C.; Iyengar, S. S.; Tomasi, J.; Cossi, M.; Rega, N.; Millam, J. M.; Klene, M.; Knox, J. E.; Cross, J. B.; Bakken, V.; Adamo, C.; Jaramillo, J.; Gomperts, R.; Stratmann, R. E.; Yazyev, O.; Austin, A. J.; Cammi, R.; Pomelli, C.; Ochterski, J. W.; Martin, R. L.; Morokuma, K.; Zakrzewski, V. G.; Voth, G. A.; Salvador, P.; Dannenberg, J. J.; Dapprich, S.; Daniels, A. D.; Farkas, O.; Foresman, J. B.; Ortiz, J. V.; Cioslowski, J.; Fox, D. J. *Gaussian 09*, Revision A.01; Gaussian, Inc.: Wallingford, CT, 2009.

DOI: 10.1021/jacs.5b05586
J. Am. Chem. Soc. 2015, 137, 11038−11046